

Article

Study on NH₃-SCR Activity and HCl/H₂O Tolerance of Titanate-Nanotube-Supported MnO_x-CeO₂ Catalyst at Low Temperature

Qiulin Wang¹, Feng Liu¹, Zhihao Wu¹, Jing Jin¹, Xiaoqing Lin^{2,*}, Shengyong Lu² and Juan Qiu³

¹ School of Energy and Power Engineering, University of Shanghai for Science and Technology, Shanghai 200093, China; wangql1987@usst.edu.cn (Q.W.); liufeng20210301@163.com (F.L.); 223370210@st.usst.edu.cn (Z.W.); alicejin001@163.com (J.J.)

² State Key Laboratory of Clean Energy Utilization, Institute for Thermal Power Engineering, Zhejiang University, Hangzhou 310027, China; lushy@zju.edu.cn

³ Research Institute of Zhejiang University, Taizhou 318000, China; qiujian@zju.edu.cn

* Correspondence: linxiaoqing@zju.edu.cn

Abstract: Manganese oxide-cerium oxide supported on titanate nanotubes (i.e., MnCe/TiNTs) were prepared and their catalytic activities towards NH₃-SCR of NO were tested. The results indicated that the MnCe/TiNT catalyst can achieve a high NO removal efficiency above 95% within the temperature range of 150–350 °C. Even after exposure to a HCl-containing atmosphere for 2 h, the NO removal efficiency of the MnCe/TiNT catalyst maintains at approximately 90% at 150 °C. This is attributed to the large specific surface area as well as the unique hollow tubular structure of TiNTs that exposes more Ce atoms, which preferentially react with HCl and thus protect the active Mn atoms. Moreover, the abundant OH groups on TiNTs serve as Brønsted acid sites and provide H protons to expel Cl atom from the catalyst surface. The irreversible deactivation caused by HCl can be alleviated by H₂O. That is because the dissociated adsorption of H₂O on TiNTs forms additional OH groups and relieves HCl poisoning.

Keywords: titanate nanotubes; manganese-cerium oxides; low-temperature deNO_x; HCl and H₂O poisoning



Citation: Wang, Q.; Liu, F.; Wu, Z.; Jin, J.; Lin, X.; Lu, S.; Qiu, J. Study on NH₃-SCR Activity and HCl/H₂O Tolerance of Titanate-Nanotube-Supported MnO_x-CeO₂ Catalyst at Low Temperature. *Catalysts* **2024**, *14*, 306. <https://doi.org/10.3390/catal14050306>

Academic Editors: Leonarda Liotta and Giuseppe Pantaleo

Received: 13 April 2024

Revised: 26 April 2024

Accepted: 29 April 2024

Published: 5 May 2024



Copyright: © 2024 by the authors. Licensee MDPI, Basel, Switzerland. This article is an open access article distributed under the terms and conditions of the Creative Commons Attribution (CC BY) license (<https://creativecommons.org/licenses/by/4.0/>).

1. Introduction

Incineration has been widely applied to dispose of municipal solid waste in China since it can reduce the volume of solid waste and allow energy recovery. Nitrogen oxide (NO_x) emissions from waste incinerators are comparable to those from fossil fuel combustion [1]. Selective catalytic reduction (SCR) with NH₃ has been proven to be an efficient post-combustion deNO_x technology and has been applied in some waste incinerators. Although the monolith V₂O₅-WO₃/TiO₂ catalyst is the most commonly used SCR catalyst, several critical issues still need to be solved. Firstly, the high and narrow active temperature window (300–400 °C) of the V₂O₅-WO₃/TiO₂ [2,3] demands additional device and extra energy to reheat the flue gas behind baghouse filter (150–170 °C) so that high NO conversion can be guaranteed [4–6]; secondly, the poor resistance of SCR catalysts to complicated flue gas compositions (e.g., SO_x, HCl and alkali metals) causes the inevitable deactivation of catalysts and increases the catalyst replacement cost; thirdly, vanadium has biological toxicity, and the final disposal of the discarded V₂O₅-WO₃/TiO₂ catalyst still remains an urgent problem. Therefore, an environmentally friendly and non-vanadium-based catalyst with excellent low-temperature activity and strong resistance needs to be developed.

Manganese oxides (MnO_x) are the most promising alternative to VO_x due to its excellent low-temperature activity towards NH₃-SCR of NO_x [7]. However, MnO_x-based catalysts are susceptible to chlorinated contaminants generated from the incineration of

various chlorine-containing wastes [8]. As reported, chlorine in wastes mainly transforms into HCl, and its concentration in raw flue gas ranges between 200 and 1500 ppm [9]. Although this value can be effectively controlled with alkaline reagents ($\text{Ca}(\text{OH})_2$ or NaHCO_3) to meet the China emission limit of 60 mg/m^3 (GB18485-2014), the residual HCl in flue gas still leads to the deactivation of MnO_x catalysts [10,11]. Cerium oxide (CeO_2) is often chosen as a promoter to enhance the low temperature activity as well as the anti-poisoning property of MnO_x [12,13]. Our previous studies [14,15] found that the combination of CeO_2 with MnO_x forms MnCeO_x solid solution and accelerates the redox cycle of the catalyst [16]. Moreover, the preferential reaction of CeO_2 with poisonous substances protects the active MnO_x species from being poisoned [13].

Catalyst support also plays an important role in the optimization and regulation of catalyst performance. Compared with other morphologies of TiO_2 (e.g., nanoparticle, nanowire, nanorod, etc.), titanium dioxide nanotubes (TiNTs) with larger specific surface areas (approximately $400 \text{ m}^2/\text{g}$) and unique hollow tubular structures have been shown to be effective in promoting low-temperature activity and enhancing the resistance property of catalysts [16–18]. In our previous study [19], we prepared a TiNT-supported $\text{MnO}_x\text{-CeO}_2$ composite and found that MnCe/TiNT catalyst exhibited higher catalytic activity within a wider temperature range of $100\text{--}400 \text{ }^\circ\text{C}$ and stronger resistance to SO_2 and H_2O . Lower levels of the harmful byproduct N_2O and higher N_2 selectivity were achieved using the TiNT-supported $\text{MnO}_x\text{-CeO}_2$ catalyst.

In this paper, a new preparation process was employed to further improve the catalytic activity and HCl/ H_2O tolerance of the MnCe/TiNT catalyst. The sol–gel method was first used to synthesize a TiO_2 -supported $\text{MnO}_x\text{-CeO}_2$ composite (denoted as MnCe/ TiO_2) to enhance the interaction between active components and support. Then, the prepared MnCe/ TiO_2 sample was subsequently transformed into the nanotube-like MnCe/TiNT catalyst using hydrothermal treatment. After that, the NH_3 -SCR activity and HCl/ H_2O tolerance of the prepared MnCe/TiNT catalysts were evaluated. Furthermore, catalytic characterizations were also conducted to clarify the promotion mechanism of TiNTs on the performance of the catalyst.

2. Results and Discussion

2.1. NH_3 -SCR Activity of the MnCe/TiNTs and MnCe/ TiO_2 Catalysts

The notations and molar ratios of the synthesized catalysts are listed in Table 1. As shown in Figure 1, the $\text{Mn}_{0.15}\text{Ce}_{0.05}/\text{TiNT}$ catalyst demonstrates the highest η_{NO} in the entire temperature range of $150\text{--}400 \text{ }^\circ\text{C}$. Its η_{NO} reaches above 98% even when the temperature is as low as $150 \text{ }^\circ\text{C}$ and can be maintained at approximately 95% in a wider temperature range of $150\text{--}350 \text{ }^\circ\text{C}$. This indicates that TiNTs can significantly improve the SCR activity and broaden the active temperature window of the catalyst. This can be attributed to the larger specific surface area and unique hollow tubular structure of TiNTs. Both of them improve the adsorption capacity of the catalyst and capture more reactant molecules for NH_3 -SCR reaction. Moreover, TiNTs achieve high dispersion of active components on the inner and outer wall of TiNTs, which enriches the number of active sites on the catalyst surface [20,21]. The above reasons explain the higher catalytic activity of MnCe/TiNTs at low temperatures.

Table 1. The notations and molar ratios of the MnCe/ TiO_2 and MnCe/TiNT catalysts.

| Notation | Component Molar Ratio | |
|---|-----------------------|-------|
| | Mn/Ti | Ce/Ti |
| $\text{Mn}_{0.15}\text{Ce}_{0.01}/\text{TiNTs}$ | | 0.01 |
| $\text{Mn}_{0.15}\text{Ce}_{0.05}/\text{TiNTs}$ | 0.15 | 0.05 |
| $\text{Mn}_{0.15}\text{Ce}_{0.10}/\text{TiNTs}$ | | 0.10 |
| $\text{Mn}_{0.15}\text{Ce}_{0.15}/\text{TiNTs}$ | | 0.15 |
| $\text{Mn}_{0.15}\text{Ce}_{0.05}/\text{TiO}_2$ | 0.15 | 0.05 |

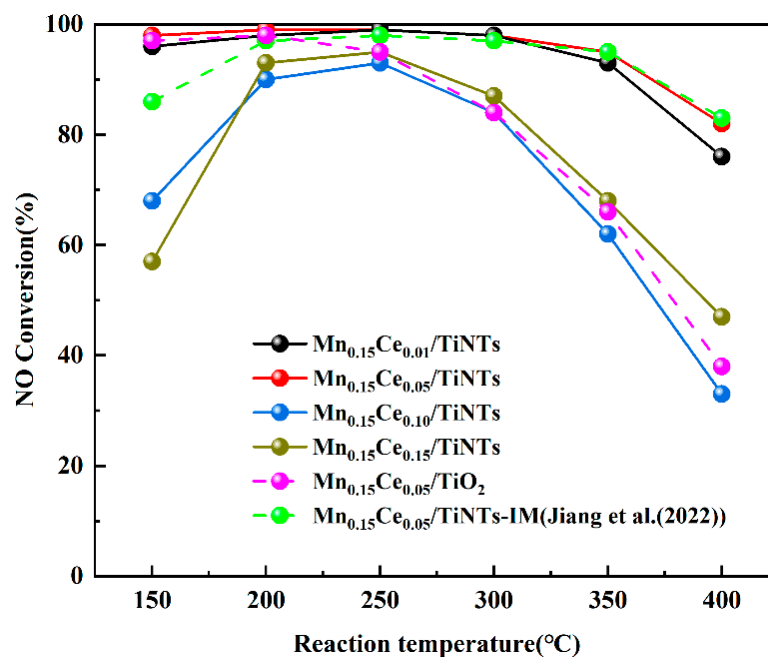


Figure 1. Catalytic activities of the MnCe/TiNTs and MnCe/TiO₂ catalysts prepared in this paper as well as the Mn_{0.15}Ce_{0.05}/TiNTs-IM catalysts prepared in ref. [19] ([NO] = [NH₃] = 500 ppm, [O₂] = 11 vol.%, N₂ as balance, GHSV = 30,000 h⁻¹).

In comparison with our previous obtained MnCe/TiNT catalyst [19], which loaded MnO_x and CeO₂ onto TiNTs using an impregnation method (denoted as Mn_{0.15}Ce_{0.05}/TiNTs-IM), the MnCe/TiNT catalyst in this paper exhibits higher catalytic activity especially at low temperature. This is because the sol-gel method was employed rather than the impregnation method to load active components in this work, effectively enhancing the interaction between Mn, Ce, O and Ti atoms, thus improving the NH₃-SCR activity of the catalyst.

An either too high or too low Ce/Ti molar ratio reduces the NH₃-SCR activity of the MnCe/TiNT catalyst, especially with an elevated Ce/Ti molar ratio. Excessively low CeO₂ content lowers its interaction with MnO_x as well as the catalyst carrier [22]. However, excessively high CeO₂ content may (1) reduce the exposure of active Mn atoms instead by incorporating most of the Mn atoms into its bulk phase [22]; (2) block the pore structures on the catalyst surface due to its agglomeration [23]; and (3) obstruct the construction of nanotubes [12]. The above factors explain the lower SCR activities of Mn_{0.15}Ce_{0.10}/TiNTs and Mn_{0.15}Ce_{0.15}/TiNT catalysts at temperatures below 200 °C. Above 250 °C, the SCR activities of these catalysts also drop dramatically. This can be ascribed to the high temperature over oxidation of NH₃ induced by excess CeO₂. Therefore, the Mn_{0.15}Ce_{0.05}/TiNT catalyst (subsequently abbreviated as MnCe/TiNTs) with the highest low temperature activity as well as the broadest active temperature window is selected for the following study.

2.2. HCl/H₂O Tolerance of the MnCe/TiNTs and MnCe/TiO₂ Catalysts

According to Figure 2, the MnCe/TiO₂ and MnCe/TiNT catalysts exhibit a high and stable η_{NO} of 98% at 150 °C for 12 h without HCl or H₂O. Their SCR activities are almost unaffected with 50 ppm HCl. As for 100 ppm and 200 ppm HCl, the η_{NO} of the MnCe/TiO₂ catalyst decreases rapidly to 70% and 45% within 2 h, respectively, while that of the MnCe/TiNT catalyst maintained at 90% and 62%. The stronger HCl tolerance of the MnCe/TiNT catalyst can be attributed to the following reasons: (1) the highly dispersed Ce atoms can react with HCl preferentially, protecting the active Mn atoms [12]; (2) TiNTs mainly exist in the form of H₂Ti₃O₇, which can provide abundant H protons for Cl atoms to leave the catalyst surface in the form of HCl [24].

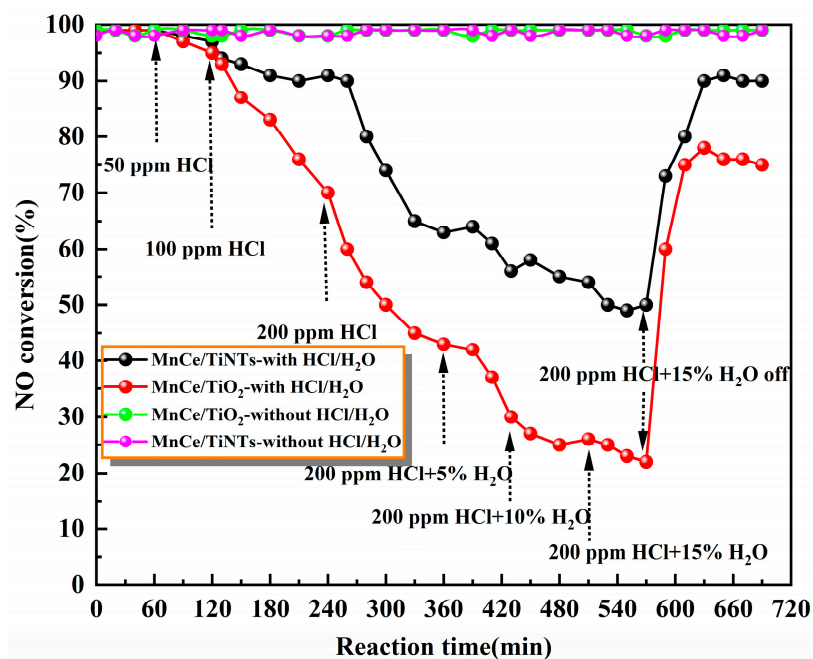


Figure 2. The HCl and H₂O tolerances of the MnCe/TiNTs and MnCe/TiO₂ catalysts.

The addition of H₂O further reduces the η_{NO} of the MnCe/TiO₂ and MnCe/TiNT catalysts at 150 °C. This is because H₂O competes with the reactants for surface adsorption sites and hinders the NH₃-SCR reaction [25]. In comparison with the MnCe/TiO₂ catalyst, the MnCe/TiNT catalyst possesses stronger HCl/H₂O tolerance; its η_{NO} can be maintained above 50% after being exposed to 200 ppm HCl and 15 vol.% H₂O for 3 h. After removing HCl and H₂O, the η_{NO} of the MnCe/TiO₂ catalyst recovers to 75% while that of the MnCe/TiNT catalyst can be restored to 90%. This result indicates that TiNTs as a support can facilitate the removal of HCl from the catalyst surface and alleviate the irreversible deactivation caused by HCl and H₂O.

2.3. Discussion Regarding the Promotion Effect of TiNTs on Catalytic Performance

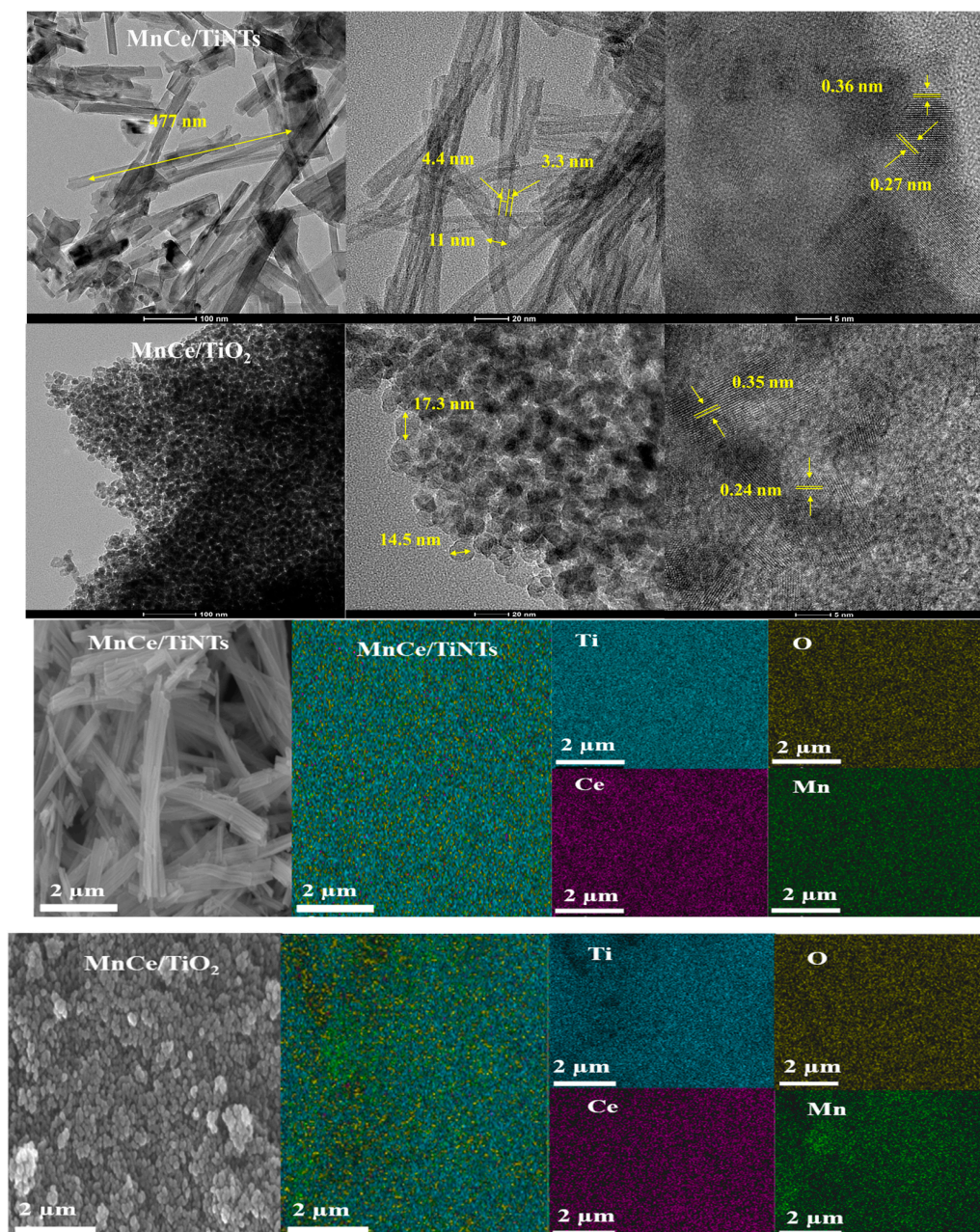
2.3.1. TEM and SEM Analysis

To clarify the promotion effect of TiNTs on catalytic performance, the MnCe/TiO₂ and MnCe/TiNT catalysts treated under different conditions (shown in Table 2) were characterized. The TEM images (Figure 3) demonstrate the unique hollow tubular structure of the MnCe/TiNT catalyst, and its outer diameter, wall thickness and tube lengths are 10–20 nm, 3–4 nm and 300–500 nm, respectively. The surface of the MnCe/TiNT catalyst was found to be smooth, indicating that Mn and Ce atoms enter the TiNTs bulk phase rather than being loaded on the surface. The overlapping of the H₂Ti₃O₇(110) lattice plane (interplanar crystal spacing = 0.36 nm) and Mn₂O₃(220) lattice plane (interplanar crystal spacing = 0.27 nm) is observed in the TEM image of the MnCe/TiNT catalyst. This observation confirms the close interaction between active components and catalyst support. The MnCe/TiO₂ catalyst exists in the form of a granular morphology with particle sizes ranging from 10 to 20 nm. The overlapping of anatase TiO₂(101) lattice plane (interplanar crystal spacing = 0.35 nm) with the MnO₂(100) lattice plane (interplanar crystal spacing = 0.24 nm) is also found, indicating the successful loading of MnO_x species on TiO₂. However, CeO₂ crystals are not detected in the TEM images, likely due either to its low content or to its incorporation with the TiNTs bulk phase [19]. In the SEM-EDS map, Mn and Ce elements are more highly dispersed on TiNTs surface compared to that on the TiO₂ surface.

Table 2. The treatment conditions and structural information of the MnCe/TiO₂ and MnCe/TiNT catalysts.

| Catalyst | Treatment Conditions | | | | S_{BET} (m ² /g) ^a | V_{tot} (cm ³ /g) ^a | D_{ave} (nm) ^a |
|-----------------------------|----------------------|------------------|-------------------------|----------------------------------|---|--|------------------------------------|
| | Time (h) | Temperature (°C) | HCl Concentration (ppm) | H ₂ O Content (vol.%) | | | |
| MnCe/TiO ₂ | / | / | / | / | 143.5 | 0.28 | 9.20 |
| MnCe/TiO ₂ -Cl | 2 | 150 | 200 | / | 79 | 0.22 | 11.2 |
| MnCe/TiO ₂ -Cl-H | 2 | 150 | 200 | 15 | 85 | 0.23 | 10.2 |
| MnCe/TiNTs | / | / | / | / | 191.7 | 0.37 | 6.64 |
| MnCe/TiNTs-Cl | 2 | 150 | 200 | / | 165.5 | 0.32 | 7.7 |
| MnCe/TiNTs-Cl-H | 2 | 150 | 200 | 15 | 166.7 | 0.33 | 7.7 |

^a S_{BET} , V_{tot} and D_{ave} represent BET specific surface area, total pore volume and average pore diameter of catalysts determined via N₂ adsorption–desorption.

**Figure 3.** The TEM and SEM-EDS images of the MnCe/TiNTs and MnCe/TiO₂ catalysts.

2.3.2. XRD and BET Analysis

According to the XRD patterns in Figure 4, the diffraction peaks corresponding to anatase (PDF#21-1272) rather than rutile TiO_2 appear in the MnCe/TiO_2 catalyst. The diffraction peaks at 37.1° and 55.1° correspond to the (100) lattice plane of MnO_2 (PDF#30-0820) and (440) lattice plane of Mn_2O_3 (PDF#41-1422), respectively [7]. The peaks belonging to the CeO_2 crystal are not detected either due to its low content or the formation of MnCeO_x solid solution [12]. As for the $\text{MnCe}/\text{TiO}_2\text{-Cl}$ catalyst, the diffraction peaks assigned to MnO_x and TiO_2 become weakened, mainly because the chlorination of the MnCe/TiO_2 catalyst distorts the crystal structures [14]. The diffraction peaks of the $\text{MnCe}/\text{TiO}_2\text{-Cl-H}$ catalyst are not further weakened, implying that the addition of H_2O barely influences the crystal structure of catalyst.

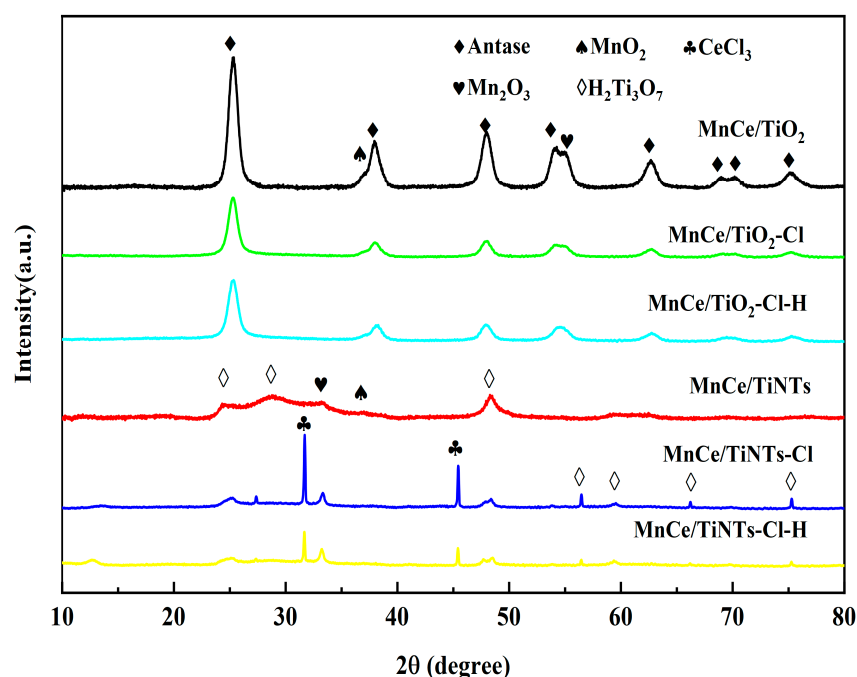


Figure 4. XRD patterns of the fresh and the treated MnCe/TiNTs and MnCe/TiO_2 catalysts.

As for the MnCe/TiNT catalyst, three main diffraction peaks at 24.5° , 27.5° and 48.5° correspond to (200), (110) and (020) lattice planes of $\text{H}_2\text{Ti}_3\text{O}_7$ (PDF#47-0561), respectively [26]. However, the intensities of these diffraction peaks are rather weak, possibly resulting from the incorporation of Mn and Ce atoms into its bulk phase, which distorts the crystal structure of TiNTs. The diffraction peak corresponding to CeCl_3 appears in the XRD pattern of the $\text{MnCe}/\text{TiNTs-Cl}$ catalyst, possibly because the highly dispersed Ce atoms react with HCl. Meanwhile, more reflections belonging to $\text{H}_2\text{Ti}_3\text{O}_7$ appear at the positions of $50\text{--}80^\circ$. This phenomenon can be attributed to the interaction between Cl atoms and TiNTs, which alters the crystal structure of TiNTs [24]. As for the $\text{MnCe}/\text{TiNTs-Cl-H}$ catalyst, the intensity of the diffraction peak corresponding to CeCl_3 is significantly weakened, confirming that the presence of H_2O can alleviate the catalytic deactivation induced by HCl [25].

Compared with the MnCe/TiO_2 catalyst, the S_{BET} and V_{tot} of the MnCe/TiNT catalyst increase from $143.5 \text{ m}^2/\text{g}$ and $0.28 \text{ cm}^3/\text{g}$ to $191.7 \text{ m}^2/\text{g}$ and $0.37 \text{ cm}^3/\text{g}$, respectively. However, those of the $\text{MnCe}/\text{TiO}_2\text{-Cl}$ catalyst decrease by 45% and 22%, while those of the $\text{MnCe}/\text{TiNTs-Cl}$ catalyst decrease by only 14%. This further proves that TiNTs can relieve the negative effect of HCl on the catalyst. The S_{BET} value of the $\text{MnCe}/\text{TiNTs-Cl-H}$ catalyst is slightly larger than that of the $\text{MnCe}/\text{TiNTs-Cl}$ catalyst, indicating that the presence of H_2O can prevent the catalyst from being destructed by HCl to some extent.

2.3.3. NH₃-TPD and H₂-TPR Analysis

NH₃-SCR reaction begins with the adsorption of NH₃ onto the surface acid sites, followed by the redox reaction between the adsorbed NH₃ with the gaseous NO or adsorbed NO [27]. Therefore, surface acidity is one of the crucial factors that determines the catalytic activity. Studies [12,28] have reported that the desorption peak at approximately 200 °C refers to the desorption of NH₄⁺ adsorbed on Brønsted acid sites (labeled as B acid sites), while the peak increases at approximately 400 °C due to the desorption of NH₃ coordinated on Lewis acidic sites (labeled as L acid sites). As shown in Figure 5a, the total number of surface acid sites on the fresh MnCe/TiNT catalyst is larger than that on the MnCe/TiO₂ catalyst. This could be attributed, on one hand, to the TiNTs being able to expose more active metal atoms to catalyst surface and increase the surface L acid sites [29]; on the other hand, TiNTs mainly exists in the form of H₂Ti₃O₇, which introduces abundant OH groups serving as B acid sites.

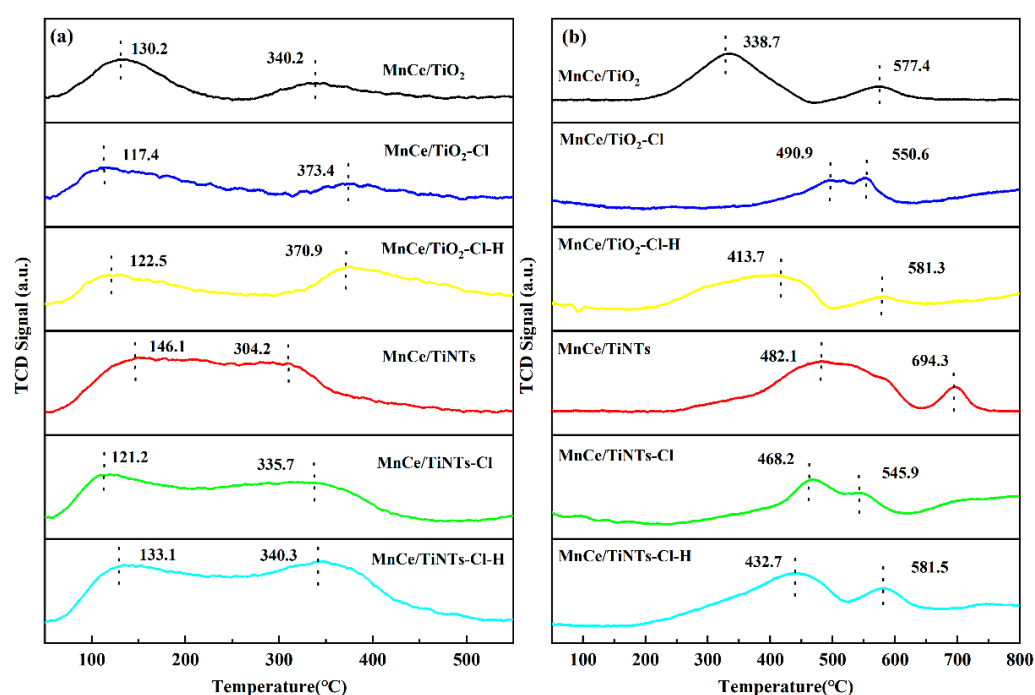


Figure 5. NH₃-TPD (a) and H₂-TPR (b) curves of the fresh and treated MnCe/TiNTs and MnCe/TiO₂ catalysts.

The number of surface acid sites on the MnCe/TiO₂-Cl catalyst is significantly reduced due to the adsorption of HCl onto the uncoordinated metal sites (M-O-M+HCl→M-OH+M-Cl) [30] as well as the interaction between HCl and surface OH groups (M-OH+HCl→M-Cl+H₂O) [31]. As for the MnCe/TiNT catalyst, the surface acidity is almost maintained after treatment with HCl. This is mainly because (1) the highly dispersed Ce atoms on the TiNTs surface can preferentially react with HCl and protect the surface active MnO_x and (2) the abundant OH groups on TiNTs surface provide more H protons to expel the adsorbed Cl atoms. However, shifts in the NH₃ desorption peaks for the MnCe/TiNTs-Cl catalyst are observed due to the reaction of HCl with surface OH group and active components, which changes the surface structure of the catalyst. The total number of surface acid sites on the MnCe/TiNTs-Cl-H catalyst was found to be even higher than that observed for the fresh catalyst, suggesting that the presence of H₂O can improve the surface acidity, alleviating HCl poisoning of the catalyst to some extent.

As shown in Figure 5b, the reduction peaks of the MnCe/TiNT catalyst are shifted to the higher temperature region in comparison with the MnCe/TiO₂ catalyst. This is possibly because the partial surface reactive oxygen species enter the nanotube and bond more

tightly to the inner walls of TiNTs, which makes it more difficult for them to be offered to oxidize H_2 . A similar result was observed in our previous study [19]. TiNTs can effectively regulate the redox ability of the catalyst, which contributes to a reduction in the excessive oxidation of NH_3 and broadens the active temperature window of the MnCe/TiNT catalyst.

As for the MnCe/TiO₂-Cl catalyst, the total area of the reduction peaks decreases and their positions are shifted to higher temperatures significantly more compared to the fresh one. This can be ascribed to the anchor of the chlorine atoms on the surface O_v, which hinders the redox cycle of the catalyst [32,33]. As for the MnCe/TiNTs-Cl catalyst, the positions remain unchanged, and their areas decline slightly. This explains the stronger resistance of the MnCe/TiNT catalyst to HCl. Furthermore, the reduction peaks of the MnCe/TiO₂-Cl-H and MnCe/TiNTs-Cl-H catalysts change less. This phenomenon confirms that the chlorination of the surface reactive components can be effectively alleviated in the presence of H₂O, especially in the case of the MnCe/TiNT catalyst.

2.3.4. TG Analysis

As reported, mass loss at 30–200 °C can be attributed to the evaporation of physically adsorbed H₂O, and that within 200–600 °C is assigned to the decomposition of the residual organic compounds on the catalyst surface [34]. Additionally, the mass loss above 600 °C occurs due to the decomposition of active components on the catalyst [35]. The MnCe/TiNT catalyst shows larger mass loss below 200 °C than the MnCe/TiO₂ catalyst (Figure 6), possibly because the greater hydrophilicity of TiNTs allows the adsorption of more H₂O molecules.

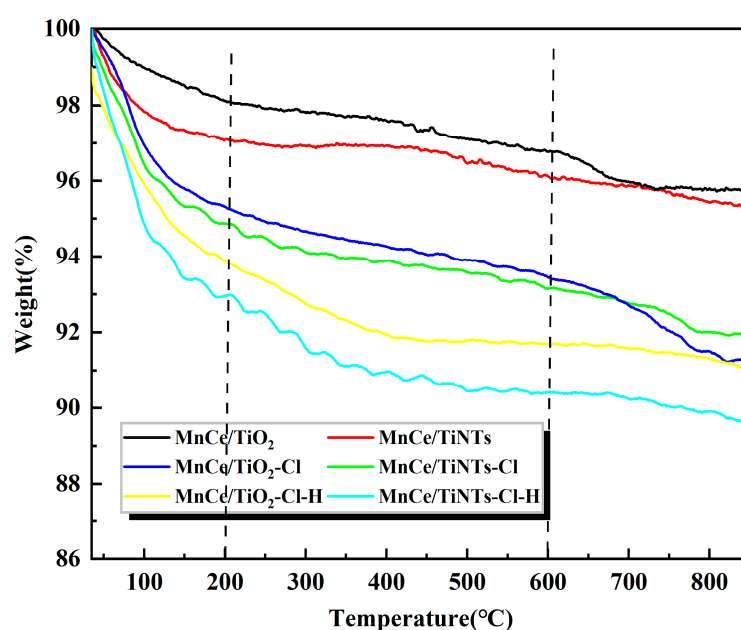


Figure 6. TG curves of the fresh and treated MnCe/TiNTs and MnCe/TiO₂ catalysts.

In comparison with the fresh MnCe/TiO₂ catalyst, more mass loss is observed below 200 °C and above 600 °C for the MnCe/TiO₂-Cl catalyst. The former can be attributed to the desorption of the weakly adsorbed HCl [36]; the latter can be ascribed to the volatilization and decomposition of metal chlorides on the catalyst surface, which is produced from the chlorination of the catalyst [37]. The mass loss of the MnCe/TiNTs-Cl catalyst above 600 °C is clearly lower than that of the MnCe/TiO₂-Cl catalyst. This confirms that TiNTs can hinder the chlorination of catalyst induced by HCl. The MnCe/TiO₂-Cl-H and MnCe/TiNTs-Cl-H catalysts exhibited significant mass loss below 600 °C, while that above 600 °C was barely observed. This further suggests that the presence of H₂O can alleviate the chlorination of catalysts.

2.3.5. XPS Analysis

The XPS spectra of the catalysts are shown in Figure 7. In the Mn 2p spectra, the peaks located at binding energies of 652.2 eV (or 640.7 eV), 653.5 eV (or 642.1 eV), and 655.3 eV (or 645.5 eV) correspond to Mn^{2+} , Mn^{3+} , and Mn^{4+} respectively. As for the Ce 3d spectra, the peaks at 904.7 eV and 885.7 eV can be assigned to Ce^{3+} , with the rest belonging to Ce^{4+} [12]. A higher Mn^{4+} content indicates a better redox ability of the catalyst, and Ce^{3+} content is regarded as an indicator of surface oxygen vacancy (O_v) [20]. As shown in Table 3, the MnCe/TiNT catalyst exhibits higher Mn^{4+} (30.8%) and Ce^{3+} (27.3%) contents, while those of the MnCe/TiO₂ catalyst are merely 26.0% and 21.7%, respectively. This is one of the main explanations for the higher catalytic activity of the MnCe/TiNT catalyst.

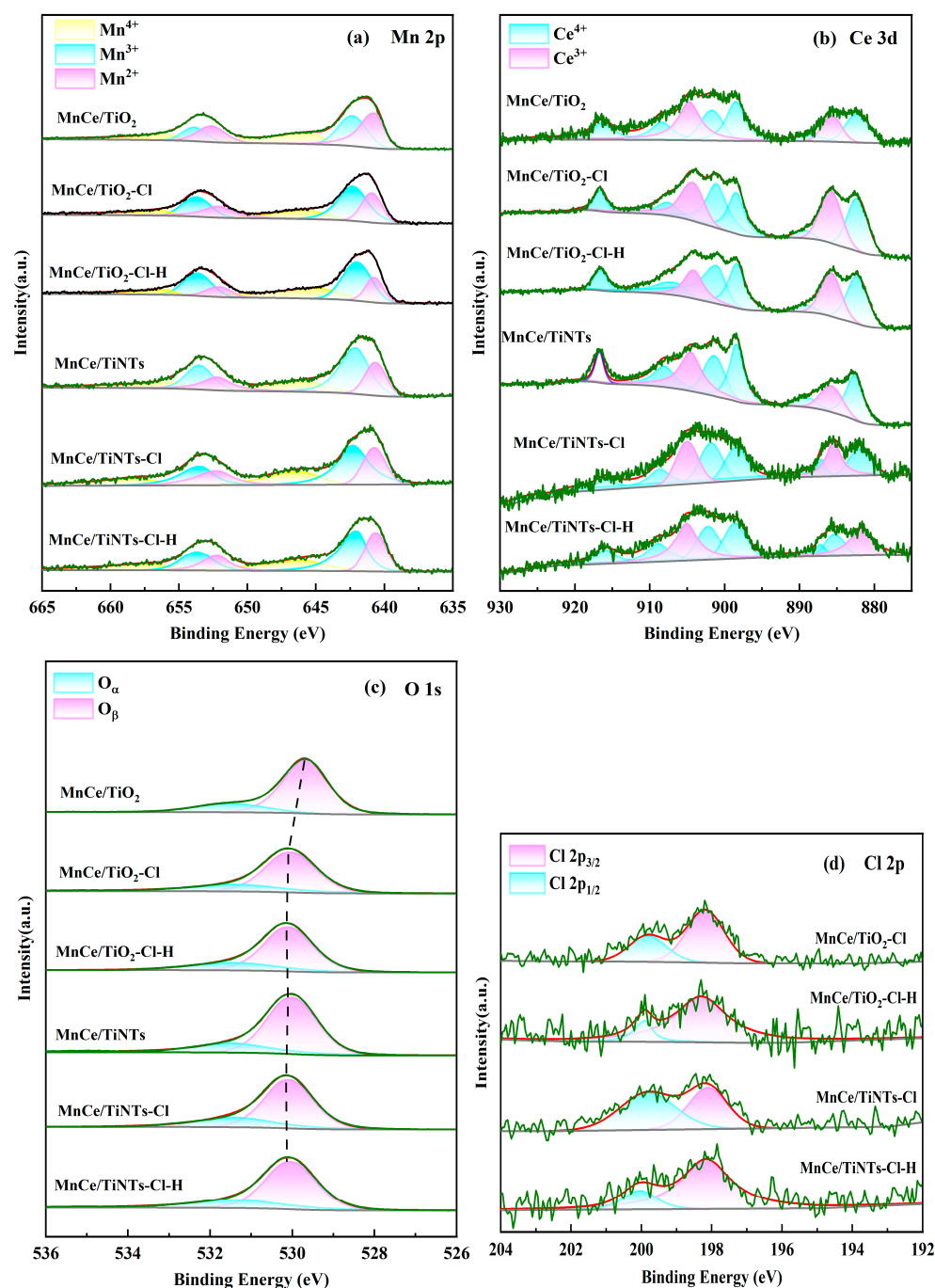


Figure 7. Mn 2p (a), Ce 3d (b), O 1s (c), and Cl 2p (d) spectra of fresh and treated MnCe/TiNTs and MnCe/TiO₂ catalysts.

Table 3. Surface element content and metal valence state distribution of the fresh and treated MnCe/TiNTs and MnCe/TiO₂ catalysts.

| Catalysts | Mn (at%) | Mn Valence Distribution (%) | | | Ce (at%) | Ce Valence Distribution (%) | | Ti (at%) | O (at%) | O _α /(O _α +O _β) | Cl (at%) |
|-----------------------------|----------|-----------------------------|------------------|------------------|----------|-----------------------------|------------------|----------|---------|---|----------|
| | | Mn ⁴⁺ | Mn ³⁺ | Mn ²⁺ | | Ce ⁴⁺ | Ce ³⁺ | | | | |
| MnCe/TiO ₂ | 3.85 | 26.0 | 47.2 | 26.8 | 1.25 | 78.3 | 21.7 | 18.46 | 50.55 | 22.4 | |
| MnCe/TiO ₂ -Cl | 2.73 | 21.8 | 46.4 | 32 | 0.97 | 83.8 | 16.2 | 18.4 | 51.78 | 18.4 | 7.0 |
| MnCe/TiO ₂ -Cl-H | 2.84 | 24.4 | 47.9 | 27.7 | 0.7 | 81.9 | 18.1 | 19.2 | 54.3 | 19.2 | 5.6 |
| MnCe/TiNTs | 2.18 | 30.8 | 31.9 | 37.3 | 0.86 | 72.7 | 27.3 | 20.74 | 51.95 | 27.5 | |
| MnCe/TiNTs-Cl | 1.34 | 28.9 | 43.7 | 27.4 | 0.63 | 76 | 24 | 22.3 | 54.2 | 25.1 | 4.8 |
| MnCe/TiNTs-Cl-H | 2.03 | 29.9 | 41.4 | 28.7 | 0.45 | 74.5 | 25.5 | 23.1 | 59.6 | 26.1 | 3.0 |

The Mn⁴⁺ and Ce³⁺ contents on the MnCe/TiO₂ catalyst decrease to 21.8% and 16.2%, respectively, resulting from the adsorption of HCl, which inhibits the redox cycle of the catalyst. The MnCe/TiNTs-Cl catalyst exhibits a smaller decrease in both Mn⁴⁺ (28.9%) and Ce³⁺ (24.0%) content, confirming that TiNTs can protect the surface-active sites and enhance the resistance of the catalyst to HCl. The Mn⁴⁺ (29.9%) and Ce³⁺ (25.5%) contents of the MnCe/TiNTs-Cl-H catalyst are almost equal to that of the fresh catalyst, further confirming that the presence of H₂O can protect the catalyst from being poisoned by HCl.

The O 1s spectra show two peaks at 531.5 eV and 530.0 eV that correspond to the surface chemisorbed oxygen (O_α) and surface reactive lattice oxygen (O_β), respectively [38]. O_α is more readily involved in the redox reactions due to its strong mobility [39]. Therefore, the O_α/(O_α+O_β) ratio is an important indicator of the catalytic activity [19]. Compared with the MnCe/TiO₂ catalyst, the MnCe/TiNT catalyst has a higher O_α/(O_α+O_β) value and the position of its O_β peak shifts to higher binding energy. Both of these factors contribute to the larger oxygen storage capacity as well as the higher surface oxygen mobility of the catalyst [19]. The O_α/(O_α+O_β) ratio of the MnCe/TiO₂-Cl catalyst is significantly lower than that of the fresh one. As for the MnCe/TiNTs-Cl catalyst, a lower reduction in the O_α/(O_α+O_β) ratio is observed, mainly because the abundant OH groups on the TiNTs surface provide H⁺ protons to expel Cl atoms in the form of HCl. The O_α/(O_α+O_β) ratios of the MnCe/TiO₂-Cl-H and MnCe/TiNTs-Cl-H catalysts are larger than those of the MnCe/TiO₂-Cl and MnCe/TiNTs-Cl catalysts. This agrees well with the above conclusion that the presence of H₂O mitigates the chlorination of the catalyst.

The contents of Cl atoms adsorbed on the catalyst surface are determined from XPS spectra, and the results are also listed in Table 3. Compared to the MnCe/TiO₂-Cl catalyst, the MnCe/TiNTs-Cl catalyst shows a significantly lower surface Cl content. This further supports the conclusion that TiNTs can reduce the adsorption of HCl on the catalyst surface. Moreover, the MnCe/TiO₂-Cl-H and MnCe/TiNTs-Cl-H catalysts show lower Cl content than the MnCe/TiO₂-Cl and MnCe/TiNTs-Cl catalysts. This also confirms that the presence of H₂O can relieve the deposition of Cl atoms on the catalyst surface.

3. Methods and Materials

3.1. Catalyst Preparation and Characterization

MnCe/TiNT catalysts were synthesized following two steps. Firstly, the MnCe/TiO₂ sample was prepared using the sol-gel method [7] using manganese nitrate, cerium nitrate and tetrabutyl titanate as precursors. Secondly, the prepared MnCe/TiO₂ sample was mixed with 10 mol/L NaOH solution and then transferred to a high-pressure hydrothermal reactor. After reacting at 150 °C for 24 h, the mixture was cooled and washed with deionized water. Subsequently, the obtained solid was aged in 0.1 mol/L HCl solution for 12 h, followed by washing with deionized water to achieve a neutral pH. Then, the sample was dried at 100 °C for 12 h and crushed to 40–60 mesh. Finally, the sample was calcined in air at 400 °C for 2.5 h to obtain the MnCe/TiNT catalyst. For comparison, the catalytic activity of the MnCe/TiO₂ sample obtained in the first step was also tested.

Several characterizations including TEM, SEM-EDS, XRD, N₂ adsorption–desorption measurements with BET analysis, EPR, NH₃-TPD, H₂-TPR, XPS, and TG/DTA were employed. The XRD patterns of the samples were measured using an XRD-6100 powder diffractometer (Shimadzu, Tokyo, Japan) with CuK α radiation ($\lambda = 0.15406$ nm). The catalyst samples were scanned over the range of 10–80° at a rate of 2°/min. SEM-EDS (MIRA3&Aztec X-Max, FEI, Hillsboro, OR, USA) was carried out at an operating voltage of 0.2 kV–30 kV. The elemental distribution of catalyst was obtained using EDS energy spectroscopy scanning. The morphologies of samples were examined using TEM (JEM-2010, Tokyo, Japan). The specific surface area and pore size distribution of the catalysts were determined at 77 K using an N₂ adsorption instrument equipped with an automated BET and pore analyzer (ASAP2020, Mike Instrument Co. Atlanta, GA, USA). Prior to the measurement, the samples were degassed in vacuum at 573 K for 3 h. XPS with Al Ka X-rays (Thermo ESCALAB 250Xi, Thermo Fisher Scientific, Wilmington, MA, USA) was employed to measure the surface atomic states of the catalysts. All the binding energies in XPS were calibrated using C1 s (284.8 eV) as a reference. H₂-TPR (Micromeritics Auto chem II 2920, Mike Instrument Co. Atlanta, GA, USA) was employed to measure the reducibility of catalysts, respectively. Prior to H₂-TPR, the catalyst samples (ca.70 mg) were pretreated in He at 300 °C for 2 h followed by cooling down to 50 °C. After that, the H₂-TPR was implemented from 100 to 700 °C at a heating rate of 10 °C/min in 10% H₂/Ar (50 mL/min). Prior to NH₃-TPD, the catalyst samples (ca.70 mg) were pretreated in He at 300 °C for 2 h followed by cooling down to 50 °C. After that, the NH₃-TPD was implemented from 100 to 700 °C at a heating rate of 10 °C/min in 10% NH₃/Ar (50 mL/min) and the NH₃ consumption was monitored using a thermal conductivity detector (TCD). TG/DTA was performed on a STA-449F3 thermal analyzer at a heating rate of 10 °C/min from room temperature to 600 °C under an air atmosphere.

3.2. Catalytic Activity Measurement

The activity evaluation of the catalysts was carried out using a quartz tube fixed-bed reactor (inner diameter \times length = 10 mm \times 500 mm), in which approximately 2.5 g (~2.0 mL) of powder catalyst within 40–60 mesh was loaded with the aid of a quartz screen. The catalyst was heated to the desired temperature (150–400 °C) using a tubular furnace equipped with an electric heating device. The simulated flue gas consisted of NO (500 ppm), NH₃ (500 ppm), O₂ (11 vol.%), HCl (50–200 ppm, when used), H₂O (5–15 vol.%, when used) and N₂ (as a balance). The total gas flow was maintained at 1000 mL/min using a mass flow controller, corresponding to a gas hourly space velocity (GHSV) of 30,000 h⁻¹. Repeat experiments were conducted to ensure the reliability of the data. The inlet (C_{in}) and outlet (C_{out}) concentrations of NO were monitored using a flue gas analyzer (Delta 2000CD-IV, MRU, Heilbronn, Germany). The NO conversion efficiency (η_{NO} , %) was calculated as follows:

$$\eta_{NO} (\%) = (C_{in} - C_{out})/C_{in} \times 100\% \quad (1)$$

4. Conclusions

In this paper, the MnCe/TiNT catalyst was prepared from the MnCe/TiO₂ catalyst using a hydrothermal method. The MnCe/TiNT catalyst with molar ratios of Mn/Ce/Ti = 0.15/0.05/1 exhibited optimal NH₃-SCR performance (above 95%) within a wide temperature window of 150–350 °C. In addition, the MnCe/TiNT catalyst demonstrated strong resistance to HCl. Its high catalytic activity as well as excellent HCl tolerance at low temperature can be attributed to several factors: (1) the large specific surface area of the TiNTs achieves high dispersion of active components on its inner and outer walls, creating more active sites for NH₃-SCR reaction and exposing more Ce atoms to preferential reaction with HCl; (2) TiNTs primarily exist in the form of H₂Ti₃O₇ and can provide abundant OH groups to serve as B acid sites; (3) the OH groups on the TiNTs surface can also provide sufficient H⁺ protons and drive the adsorbed Cl atoms away from the catalyst surface

in the form of HCl. The presence of H₂O reduces the NO_x removal efficiency, while the irreversible deactivation caused by HCl can be effectively alleviated with the addition of H₂O, especially for the MnCe/TiNT catalyst. Therefore, TiNTs represent an effective support to enhance the low-temperature deNO_x activity as well as the resistance of the MnO_x-CeO₂ composite to HCl and H₂O and have the potential to be further improved in the future study.

Author Contributions: Conceptualization, Q.W. and X.L.; Methodology, Q.W., X.L. and S.L.; Formal analysis, F.L. and Z.W.; Investigation, F.L., Z.W. and J.Q.; Resources, Q.W., J.J., X.L. and S.L.; Data curation, F.L.; Writing—original draft, F.L.; Writing—review & editing, Q.W.; Visualization, F.L.; Supervision, Q.W., J.J., X.L. and S.L.; Project administration, X.L.; Funding acquisition, Q.W., X.L. and S.L. All authors have read and agreed to the published version of the manuscript.

Funding: This research is supported by the Shanghai Committee of Science and Technology (23010503500).

Data Availability Statement: The original contributions presented in the study are included in the article, further inquiries can be directed to the corresponding author/s.

Conflicts of Interest: The authors declare no conflict of interest.

References

1. Li, J.H.; Chang, H.Z.; Ma, L.; Hao, J.M.; Yang, R.T. Low-temperature selective catalytic reduction of NO_x with NH₃ over metal oxide and zeolite catalysts—A review. *Catal. Today* **2011**, *175*, 147–156. [[CrossRef](#)]
2. Zengel, D.; Stehle, M.; Deutschmann, O.; Casapu, M.; Grunwaldt, J.D. Impact of gas phase reactions and catalyst poisons on the NH₃-SCR activity of a V₂O₅-WO₃/TiO₂ catalyst at pre-turbine position. *Appl. Catal. B Environ.* **2021**, *288*, 119991. [[CrossRef](#)]
3. Yates, M.; Martín, J.A.; Martín, L.; Suárez, S.; Blanco, J. N₂O formation in the ammonia oxidation and in the SCR process with V₂O₅-WO₃ catalysts. *Catal. Today* **2005**, *107–108*, 120–125. [[CrossRef](#)]
4. Li, Y.; Cheng, H.; Li, D.Y.; Qin, Y.S.; Xie, Y.M.; Wang, S.D. WO₃/CeO₂—ZrO₂, a Promising Catalyst for Selective Catalytic Reduction (SCR) of NO_x with NH₃ in diesel exhaust. *Chem. Commun.* **2008**, *39*, 1470–1472. [[CrossRef](#)] [[PubMed](#)]
5. Wang, H.J.; Huang, B.C.; Yu, C.L.; Lu, M.J.; Huang, H.; Zhou, Y.L. Research progress, challenges and perspectives on the sulfur and water resistance of catalysts for low temperature selective catalytic reduction of NO_x by NH₃. *Appl. Catal. A Gen.* **2019**, *588*, 117207. [[CrossRef](#)]
6. Song, H.; Zhang, M.L.; Yu, J.P.; Wu, W.H.; Qu, R.Y.; Zheng, C.H.; Gao, X. The Effect of Cr Addition on Hg⁰ Oxidation and NO Reduction over V₂O₅/TiO₂ Catalyst. *Aerosol Air Qual. Res.* **2017**, *18*, 803–810. [[CrossRef](#)]
7. Lin, F.; Wang, Q.L.; Zhang, J.C.; Jin, J.; Lu, S.Y.; Yan, J.H. Mechanism and Kinetics Study on Low-Temperature NH₃-SCR Over Manganese–Cerium Composite Oxide Catalysts. *Ind. Eng. Chem. Res.* **2019**, *58*, 22763–22770. [[CrossRef](#)]
8. Wang, H.S.; Liang, H.S.; Chang, M.B. Chlorobenzene oxidation using ozone over iron oxide and manganese oxide catalysts. *J. Catal.* **2011**, *186*, 1781–1787. [[CrossRef](#)]
9. Zhan, M.X.; Ji, L.J.; Ma, Y.F.; Chen, W.R.; Lu, S.Y. The impact of hydrochloric acid on the catalytic destruction behavior of 1,2-dichlorobenzene and PCDD/Fs in the presence of VWTi catalysts. *Waste. Manage.* **2018**, *78*, 249–257. [[CrossRef](#)]
10. Krishnamoorthy, S.; Amiridis, M.D. Kinetic and in situ FTIR studies of the catalytic oxidation of 1,2-dichlorobenzene over V₂O₅/Al₂O₃ catalysts. *Catal. Today* **1999**, *51*, 203–214. [[CrossRef](#)]
11. Amrute, A.P.; Mondelli, C.; Moser, M. Performance, structure, and mechanism of CeO₂ in HCl oxidation to Cl₂. *J. Catal.* **2012**, *286*, 287–297. [[CrossRef](#)]
12. Wang, Q.L.; Zhou, J.J.; Zhang, J.C.; Zhu, H.; Feng, Y.H.; Jin, J. Effect of Ceria Doping on the Catalytic Activity and SO₂ Resistance of MnO_x/TiO₂ Catalysts for the Selective Catalytic Reduction of NO with NH₃ at Low Temperatures. *Aerosol Air Qual. Res.* **2020**, *20*, 477–488. [[CrossRef](#)]
13. Fang, X.; Liu, Y.J.; Cheng, Y.; Cen, W.L. Mechanism of Ce-Modified Birnessite-MnO₂ in Promoting SO₂ Poisoning Resistance for Low-Temperature NH₃-SCR. *ACS Catal.* **2021**, *11*, 4125–4135. [[CrossRef](#)]
14. Wang, Q.L.; Lin, F.; Zhou, J.J.; Zhang, J.C.; Jin, J. Effect of HCl and o-DCBz on NH₃-SCR of NO over MnO_x/TiO₂ and MnO_x-CeO₂/TiO₂ catalysts. *Appl. Catal. A Gen.* **2020**, *605*, 117801. [[CrossRef](#)]
15. Wu, Z.B.; Jin, R.B.; Wang, H.Q.; Liu, Y. Effect of ceria doping on SO₂ resistance of Mn/TiO₂ for selective catalytic reduction of NO with NH₃ at low temperature. *Catal. Commun.* **2009**, *10*, 935–939. [[CrossRef](#)]
16. Nam, K.B.; Kwon, D.W.; Hong, S.C. DRIFT study on promotion effects of tungsten-modified Mn/Ce/Ti catalysts for the SCR reaction at low-temperature. *Appl. Catal. A Gen.* **2017**, *542*, 55–62. [[CrossRef](#)]
17. Wang, P.L.; Wang, H.Q.; Chen, X.B.; Liu, Y.; Weng, X.L.; Wu, Z.B. Novel SCR catalyst with superior alkaline resistance performance: Enhanced self-protection originated from modifying protonated titanate nanotubes. *J. Mater. Chem. A* **2014**, *3*, 680–690. [[CrossRef](#)]
18. Xiong, L.Y.; Zhong, Q.; Chen, Q.Q.; Zhang, S.L. TiO₂ nanotube-supported V₂O₅ catalysts for selective NO reduction by NH₃. *Korean J. Chem. Eng.* **2013**, *30*, 836–841. [[CrossRef](#)]

19. Jiang, Z.P.; Wang, Q.L.; Cai, Y.Z. Enhanced Catalytic Activity and SO₂/H₂O Tolerance for Selective Catalytic Reduction of NO_x with NH₃ over Titanate Nanotubes Supported MnO_x-CeO₂ Catalyst at Low Temperature. *Catal. Surv. Asia*. **2022**, *26*, 161–173. [[CrossRef](#)]
20. Wang, Z.H.; Jiao, M.Y.; Chen, Z.P.; He, H.; Liu, L.C. Effects of montmorillonite and anatase TiO₂ support on CeO₂ catalysts during NH₃-SCR reaction. *Micropor Mesopor Mat.* **2021**, *320*, 111072. [[CrossRef](#)]
21. Andreoli, S.; Deorsola, F.A.; Pirone, R. MnO-CeO₂ catalysts synthesized by solution combustion synthesis for the low-temperature NH₃-SCR. *Catal. Today*. **2015**, *253*, 199–206. [[CrossRef](#)]
22. Tang, C.J.; Li, J.C.; Yao, X.J.; Sun, J.F.; Cao, Y. Mesoporous NiO-CeO₂ catalysts for CO oxidation: Nickel content effect and mechanism aspect. *Appl. Catal. A Gen.* **2015**, *494*, 77–86. [[CrossRef](#)]
23. Zhao, X.Y.; Ma, S.B.; Li, Z.B.; Yuan, F.L.; Niu, X.Y.; Zhu, Y.J. Synthesis of Ce_nTiO_x flakes with hierarchical structure and its enhanced activity for selective catalytic reduction of NO_x with NH₃. *Chem. Eng. J.* **2020**, *392*, 123801. [[CrossRef](#)]
24. Li, C.; Hess, F.; Djerdj, I.; Chai, G.; Sun, Y.; Guo, Y.; Smarsly, B.M.; Over, H. The stabilizing effect of water and high reaction temperatures on the CeO₂-catalyst in the harsh HCl oxidation reaction. *J. Catal.* **2018**, *357*, 257–262. [[CrossRef](#)]
25. Xiong, S.C.; Liao, Y.; Xiao, X.; Dang, H.; Yang, S.J. The mechanism of the effect of H₂O on the low temperature selective catalytic reduction of NO with NH₃ over Mn-Fe spinel. *Catal. Sci. Technol.* **2015**, *5*, 2132–2140. [[CrossRef](#)]
26. Aguilar, R.M.; Camposeco, R.; Castillo, S.; Marín, J.; Rodríguez, G.V.; García, S.L.; Mejía, C.I. Acidity, surface species, and catalytic activity study on V₂O₅-WO₃/TiO₂ nanotube catalysts for selective NO reduction by NH₃. *Fuel* **2017**, *198*, 123–133. [[CrossRef](#)]
27. Ye, B.; Kim, J.; Lee, M.J.; Chun, S.Y.; Jeong, B.; Kim, T.; Lee, D.H.; Kim, H.D. Mn-Ce oxide nanoparticles supported on nitrogen-doped reduced graphene oxide as low-temperature catalysts for selective catalytic reduction of nitrogen oxides. *Micropor. Mesopor. Mat.* **2021**, *310*, 110588. [[CrossRef](#)]
28. Yang, N.Z.; Guo, R.T.; Pan, W.G. The deactivation mechanism of Cl on Ce/TiO₂ catalyst for selective catalytic reduction of NO with NH₃. *Appl. Surf. Sci.* **2016**, *378*, 513–518. [[CrossRef](#)]
29. Chen, X.B.; Wang, P.L.; Fang, P. Tuning the property of Mn-Ce composite oxides by titanate nanotubes to improve the activity, selectivity and SO₂/H₂O tolerance in middle temperature NH₃-SCR reaction. *Fuel Process Technol.* **2017**, *167*, 221–228. [[CrossRef](#)]
30. Maupin, I.; Pinard, L.; Mijoin, J.; Magnoux, P. Bifunctional mechanism of dichloromethane oxidation over Pt/Al₂O₃:CH₂Cl₂ disproportionation over alumina and oxidation over platinum. *J. Catal.* **2012**, *291*, 104–109. [[CrossRef](#)]
31. Lopez, N.; Segura, J.G.; Marin, R.P.; Ramirez, J.P. Mechanism of HCl oxidation (Deacon process) over RuO₂. *J. Catal.* **2008**, *255*, 29–39. [[CrossRef](#)]
32. Wu, Z.B.; Jin, R.B.; Liu, Y.; Wang, H.Q. Ceria modified MnO_x/TiO₂ as a superior catalyst for NO reduction with NH₃ at low-temperature. *Catal. Commun.* **2008**, *9*, 2217–2220. [[CrossRef](#)]
33. Zuo, S.F.; Huang, Q.Q.; Li, J.; Zhou, R.X. Promoting effect of Ce added to metal oxide supported on Al pillared clays for deep benzene oxidation. *Appl. Catal. B Environ.* **2009**, *91*, 204–209. [[CrossRef](#)]
34. Wu, X.; Lee, H.R.; Liu, S.; Weng, D. Sulfur poisoning and regeneration of MnO_x-CeO₂ Al₂O₃ catalyst for soot oxidation. *J. Rare Earth.* **2012**, *30*, 659–694. [[CrossRef](#)]
35. Wang, Q.L.; Huang, X.N.; Feng, Y.H. Interaction Mechanism Study on Simultaneous Removal of 1,2-Dichlorobenzene and NO over MnO_x-CeO₂/TiO₂ Catalysts at Low Temperatures. *Ind. Eng. Chem. Res.* **2021**, *60*, 4820–4830. [[CrossRef](#)]
36. Dai, Q.; Wang, X.Y.; Lu, G.Z. Low-temperature catalytic destruction of chlorinated VOCs over cerium oxide. *Catal. Commun.* **2007**, *8*, 1645–1649. [[CrossRef](#)]
37. Dai, Y.; Wang, X.Y.; Dai, Q.Y.; Li, D. Effect of Ce and La on the structure and activity of MnO_x catalyst in catalytic combustion of chlorobenzene. *Appl. Catal. B Environ.* **2012**, *111–112*, 141–149. [[CrossRef](#)]
38. Zhang, J.H.; Li, Y.B.; Wang, L.; Zhang, C.B.; He, H. Catalytic oxidation of formaldehyde over manganese oxides with different crystal structures. *Catal. Sci. Technol.* **2015**, *5*, 2305–2313. [[CrossRef](#)]
39. Boningari, T.; Ettireddy, P.R.; Somogyvari, A.; Liu, Y.; Vorontsov, A.; McDonald, C.A.; Smirniotis, P.G. Influence of elevated surface texture hydrated titania on Ce-doped Mn/TiO₂ catalysts for the low-temperature SCR of NO_x under oxygen-rich conditions. *J. Catal.* **2015**, *325*, 145–155. [[CrossRef](#)]

Disclaimer/Publisher's Note: The statements, opinions and data contained in all publications are solely those of the individual author(s) and contributor(s) and not of MDPI and/or the editor(s). MDPI and/or the editor(s) disclaim responsibility for any injury to people or property resulting from any ideas, methods, instructions or products referred to in the content.